PCCP

Multi-scale Simulation of Proton Diffusion in Dislocation Cores in $BaZrO_3$

Journal:	*Physical Chemistry Chemical Physics*
Manuscript ID	CP-ART-07-2022-002989.R3
Article Type:	Paper
Date Submitted by the Author:	24-Aug-2022
Complete List of Authors:	Yue, Shaofeng; Harbin Institute of Technology, Zhao, Junqing; Harbin Institute of Technology Sun, Yi; Harbin Institute of Technology Niu, Hongwei; Harbin Institute of Technology Li, Huyang; Harbin Institute of Technology Jing, Yuhang; Harbin Institute of Technology, Department of Astronautical Science and Mechanics Aluru, N.; The University of Texas at Austin

SCHOLARONE™
Manuscripts

Multi-scale Simulation of Proton Diffusion in Dislocation Cores in $BaZrO_3$

Shaofeng Yue[a], Junqing Zhao[a], Yi Sun[a], Hongwei Niu[a], Huyang Li[a], Yuhang Jing[a,*], N. R. Aluru[b]

[*]Corresponding author.
E-mail address: jingyh@hit.edu.cn (Y. Jing)

[a] Department of Astronautical Science and Mechanics, Harbin Institute of Technology, Harbin, Heilongjiang 150001, P. R. China

[b] Walker Department of Mechanical Engineering, Oden Institute for Computational Engineering and Sciences, The University of Texas at Austin, Austin, TX 78712, USA

Abstract

Dislocations are important for their effects on the chemical, electrical, magnetic, and transport properties of oxide materials, especially for electrochemical devices such as solid fuel cells and resistive memories, but these effects are still under-studied at the atomic level. We have developed a quantum mechanical/molecular mechanical (QM/MM)-based multiscale simulation program to reveal the diffusion properties of protons on <100> edge dislocations in $BaZrO_3$ perovskite oxide. We find that the large free space and the presence of hydrogen bonds in the dislocation core structure lead to significant trapping of protons. The diffusion properties of protons in dislocation cores were investigated, and no evidence of pipeline diffusion was found from the calculated migration energy barriers, which not only did not accelerate ion diffusion but rather decreases the conductivity of ions. The proton diffusion properties of Y-doped $BaZrO_3$ (BZY), with a dislocation core structure (BZY-D) and with a grain boundary structure (BZY-GB) were also compared. In all three structures, local lattice deformation occupies an essential part in the proton transfer and rotation processes. The change in bond order is calculated and it is found that the interaction with oxygen and Zr ions during proton transfer and rotation controls the energy barrier for local lattice deformation of the O-B-O motion, which affects the proton diffusion in the structure. Our study provides insight into proton diffusion in dislocations in terms of mechanical behavior, elucidates the origin of the energy barrier associated with proton diffusion in dislocations, and provides guidance for the preparation and application of proton conductors.

Keywords: Dislocations, Energy barrier, Proton diffusion, Multiscale simulation, Lattice deformation

1. Introduction

Barium zirconate based perovskite ceramic materials have been active in the study of solid oxide fuel cell electrolytes due to their excellent chemical stability and high ionic conductivity[1-3]. Yttrium-doped barium zirconate ($BaZr_{1-2\delta}Y_{2\delta}O_{3-\delta}$, BZY) is a typical class of solid electrolyte in which the zirconium ions (Zr^{4+}) in the original lattice are replaced by large-radius, low-charge yttrium ions (Y^{3+}), forming oxygen vacancy defects ($V_O^{\bullet\bullet}$). BZY materials can also form interstitial point defects[4, 5], line defects (edge dislocations)[6], and surface defects (grain boundaries)[7, 8] when subjected to actual hydrothermalization, high temperature sintering, or stress. Currently, experimental studies on the structure and diffusion properties of BZY defects are mostly focused on point defects, using scanning electron microscopy, electrochemical impedance spectroscopy, X-ray diffraction and other methods to investigate the effects of material structure, dopant type, concentration and local structure on carrier diffusion[9-11], while the effect of grain boundaries on ion transport properties has been investigated in a few studies[7, 12]. In addition, simulations related to BZY focus on its vacancy formation energy, carrier jump barrier, interaction with dopant ions and identification of diffusion paths[13-16].Dislocations, a prevalent defect in crystalline materials[17-19], significantly affect the material performance of solid oxide fuel cells (SOFCs)[20].

Currently, only a small number of studies have explored the chemical[21, 22], electrical[23, 24] and transport[25] properties of dislocations on oxides at the local level. Experiments have shown that dislocation-piping in metallic materials with edge-dislocation defects accelerates ion transport and increases the ion diffusion coefficient by several orders of magnitude[6, 26]. Moreover, dislocation-piping has a significant impact on the electrochemical and magnetic properties of metallic materials[27]. However, in perovskite materials such as $SrTiO_3$ and CeO_2, the dislocation defects have the opposite effect on the ion transport properties, instead of accelerating ion diffusion, they reduce the ion conductivity[28-30]. The mechanism of action of the edge dislocation defects at the atomic/molecular level is still unclear. Therefore, exploring the mechanism of proton transport in BZY materials with line defects is essential for understanding the defect structure and its role in macroscopic migration behavior, as well as providing theoretical basis and design solutions for the application of BZY-based proton conductor materials.

Density functional theory (DFT) has been successfully employed to study ion diffusion in perovskite materials, taking into account the principle of interaction between nuclei and electrons and their fundamental laws of motion, with good agreement between computational accuracy and experimental values[31-34]. However, it is very difficult to model complete dislocation defects at the DFT level, and there are few theoretical studies on the use of DFT to study proton diffusion in dislocations. Due to the symmetry breaking in the unitary dislocations, periodic boundary conditions (PBC) cannot be used in the DFT calculations. However, both free and fixed boundaries introduce virtual displacement fields to the dislocations if a clustering model is used, leading to errors in the dynamic studies. It is possible to fix the boundary mismatch by introducing another dislocation with the opposite Burgers vector, which makes it possible to apply the PBC again. However, this leads to the necessity of using larger models in the calculations, making the computational cost of using DFT for dynamics studies too high. Molecular dynamics (MD) simulations are employed to study the state of particle motion and interactions in a system over a period of time, and have been widely used to study ion diffusion in perovskite materials[35, 36]. Stokes and Islam used MD simulations in combination with Coulomb and Buckingham potentials to study the interaction between point defects and dopants in $BaZrO_3$ and $BaPrO_3$ as well as the migration characteristics of oxygen ions[37]. In addition, the interaction between the edge dislocations and $V_{\ddot{O}}$ in $SrTiO_3$ at high temperature and $MgSiO_3$ at high pressure and its effect on the oxygen diffusion kinetics were investigated by the MD method[38, 39]. The MD method ignores the quantum effects brought about by electron motion and suffers a certain degree of loss in actuarial accuracy, but has advantages in computational efficiency and computational scale that are unmatched by first-principles methods. Therefore, a multiscale scheme combining DFT and MD simulations is expected to solve the problem of proton diffusion on dislocation cores.

In this work, we developed QM/MM multiscale simulation framework to study the diffusion dynamics of protons on BZY misaligned cores. This multiscale strategy significantly reduces the computational effort while maintaining accuracy at the DFT level[40, 41]. We found that a significant proton capture effect exists when the proton diffuses in the dislocation core, the proton forms an O-H bond with oxygen ion which prefers the position with larger free space, while a stronger hydrogen bond makes the proton more stable and more likely to cause an effective proton capture. In perovskite type materials with edge dislocation defects, no dislocation-pipeline effect similar to the accelerated ion transport in metallic materials is formed. In addition, the structural disorder

on the dislocation core leads to a stronger bond between O-B for proton transfer and between O-A for proton rotation, and this leads to an increased energy barrier to O-B-O motion, which hinders proton migration in the dislocation core. Here we paper investigates the proton trapping effect in dislocation cores, the dislocation-pipeline effect in perovskite type materials, and the quantification of the activation energy source for proton transfer and rotation in BZY-D, providing a fundamental theory for industrial applications of perovskite oxides.

2. Calculation Details

The QM/MM multiscale approach, which combines quantum mechanical simulations with classical atomic simulations, was originally developed in the context of enzymatic reactions[42] and has since been widely used to help understand physical[43, 44], chemical[45, 46], and biological[47, 48] processes in complex environments. The application of the method to condensed-phase chemical reactions[49] and the development of open boundaries[50] are described in detail. The accuracy and efficiency of this multiscale scheme was demonstrated in the bulk and screw dislocations of aluminum by introducing the multiscale approach for the treatment of simple metallic systems[40]. Despite the success of this approach, the force mismatch and virtual surface effects at the DFT/MD boundary cannot be completely cancelled, which can lead to considerable errors introduced in the atomic positions and reduce the coupling at the boundary. The reconstruction method was further modified to enhance the coupling between the QM and MM regions[41]. The diffusion behavior of lithium impurities in the presence of dislocations in silicon was investigated using QM/MM theory by code-linking the SIESTA and LAMMPS packages[51, 52]. This multiscale approach was recently used to investigate how cracks affect the distribution and diffusion behavior of lithium in silicon anodes[53]. As shown in Fig.1, a region composed of several layers of B-atoms near the boundary is introduced between the QM and MM regions. The positions of the B-atoms are determined by the force field calculation in the MD and also appear as boundary atoms in the DFT calculation region I. They act as buffers to protect the internal DFT atoms from exposure to the virtual surface at the boundary, and this approach is more suitable for calculating lattice cross sections containing defects.

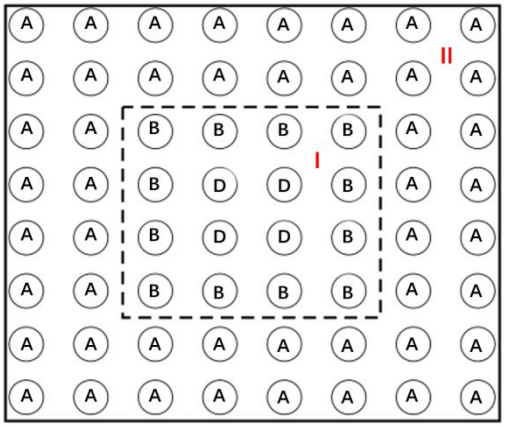

Figure 1: The division diagram of region I and region II in the multiscale approach. The atoms marked with 'D' indicate internal DFT atoms or core atoms with defects. Atoms marked with 'A' denote external MD atoms. Atoms marked with 'B' indicate boundary atoms.

In this paper, we choose to construct a BZY system with two symmetric line defect structures to ensure that the simulated system is large enough to form edge dislocations and that the structure is periodically symmetric. Firstly, the structure file of pure phase BZO (space point group $Pm\bar{3}m$, cubic lattice parameter 4.256 Å)[54] was obtained from the crystal database, and the BZO supercell was oriented in the [011] [100] [011] direction along

the slip plane <100>{011}. A 27×38×2 BZO supercell was constructed to obtain the bulk BZO model with x, y and z dimensions of11.402, 16.047 and 0.844 nm, respectively, with periodic boundary conditions along the z-axis direction; then, the middle two columns of BaO and ZrO_2 lattices (A total of 32 $BaZrO_3$) are dug out along the z-axis, after preliminary MD relaxation, dislocation dipoles are produced that have opposite Burgers vectors and are positioned as far away as possible to reduce internal interactions[51]. The 3D structure matrix of the BZY-D model is shown in Fig.2(a). The whole model includes 10,100 atoms and has two parts.:

(i) The QM region, which includes the dislocated cores, inserted protons, and boundary H-atoms, calculated in the DFT package;

(ii) The MM region, for the rest, is described by the empirical interatomic potential.

The B atoms in the atomic structure of region I is used as the boundary atoms, and these atoms are calculated jointly by DFT and MD simulations, an approach that eliminates fictitious surface effects and force mismatches between the QM and MM regions. Near the QM region the suspended bonds are passivated by H atoms. The suspended bonds near the QM region are passivated by H atoms, and the two parts of the structure are shown in Fig.2. In all models of this paper, Zr, H, Ba and O ions are marked in light blue, gray, green and red, respectively.

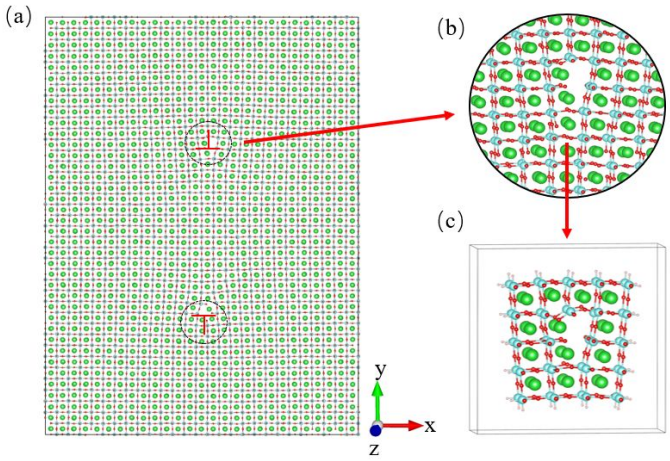

Figure 2: The dislocation models used throughout the multiscale calculations. (a) MD computational model; (b) structure near the dislocation core; (c) DFT computational model.

The DFT calculations in part (i) are performed using the Vienna Ab initio simulation package (VASP) code[55-57]. Under the generalized gradient approximation (GGA)[58, 59], the electronic wave function is described by the Blochl's projection augmentation wave (PAW) method[60, 61], using the Perdew-Burke-Ernzerhof (PBE) parameter exchange correlation energy[58]. In all calculations, the cut-off energy of the plane wave group is 500 eV, and this is already widely used to study proton migration processes in perovskites[62, 63]. After optimization, the residual force per atom is less than 0.02 eV/A. The Bader charge calculation method is used to analyze the electronic structure near the dislocation structure. The energy barrier for proton diffusion is calculated by the climbing image nudge elastic band (CI-NEB) method[64], We used three images between initial and final state during each CI-NEB calculation. The overlapping electron density of the atomic structures was calculated using the DDEC6 method[65]. In addition, all structures use a 6 × 6 × 6 Monkhorst-Pack k-point grid. The Gaussian Smearing method is used, and the width of the smearing in 0.2 eV. The relaxation of the electronic degrees of

freedom stops if the total (free) energy change and the band-structure-energy change ('change of eigenvalues') between two steps are both smaller than EDIFF= 1.0E-4 eV; Also, the relaxation stops when the norm of all forces is less than the absolute value of EDIFFG = -0.04 eV/A.

Part (ii) and the boundary atoms were calculated using the LAMMPS code. The BZY system is an inorganic ionic compound whose interactions between ions are described using the Coulomb-Buckingham potential function [66, 67] in the form of Eq. 1, where the force field potential parameters A_{ij}, ρ_{ij} and C_{ij} for different ion pairs are shown in Table 1. In the MD simulation system of BZY, the Nosé-Hoover algorithm was used to regulate the temperature and pressure; the velocity Verlet algorithm was used for data integration with a 1 fs time step; the PPPM algorithm was used for the long-range forces in K-space with a truncation radius of 12 Å; the energy minimization was performed by the fastest descent algorithm, and the convergence of the energy during relaxation was criterion is 10^{-6} and the convergence criterion for the force is 10^{-8}.

$$V_{ij} = \frac{q_i q_j}{4\pi\varepsilon_0 r_{ij}} + A_{ij} e^{-\frac{r_{ij}}{\rho_{ij}}} - \frac{C_{ij}}{r_{ij}^6} \quad (1)$$

Table 1 Potential parameters of Buckingham

Interaction	A_{ij}(eV)	ρ_{ij}(Å)	C_{ij}(eV Å^6)	Ref.
$Ba^{2+}\cdots O^{2-}$	931.700	0.3949	0.000	[67]
$Zr^{4+}\cdots O^{2-}$	985.869	0.3760	0.000	[67]
$Y^{3+}\cdots O^{2-}$	4121.837	0.2804	0.000	[66]
$O^{2-}\cdots O^{2-}$	22764.300	0.1490	27.890	[67]

3. Results and discussion

3.1 Diffusion paths of proton in dislocation core

A necessary condition for fast proton transport is the integrity and continuity of the proton diffusion path. The long-range proton conduction is crucial for the application of BZO in electrolytes, and we can obtain high proton conductivity only when protons are able to transport freely in the dislocation core. Protons in perovskite oxides usually diffuse in a Grotthuss mechanism, which includes proton transfer between two adjacent oxide ions belonging to the same BO_6-octahedron (intra-octahedral proton transfer) or between two adjacent oxide ions belonging to two BO_6-octahedra (inter-octahedral proton transfer) and hydroxide ion rotation[68-70]. The detailed steps for each of proton transfer and proton rotation are given in Fig.3. With crossing the dislocation core as a criterion, we find four typical proton diffusion paths in BZY-D consisting of a combination of proton transfer and rotation. The four diffusion paths of protons in BZY-D are given in Fig.4. Proton diffusion is composed of different permutations and combinations of proton transfer and rotation. In the diagram, the straight blue arrows indicate proton transfer and the curved orange arrows indicate proton rotation. The path in Fig.4e is the longest and contains the most complex proton diffusion process, but when the proton is near the oxygen ion involved in the fg and gh steps, it prefers to diffuse toward the oxygen ion pointed by the black arrow in Fig.4d, resulting in the proton being trapping and unable to continue diffusion. The path in Fig.4f is the shortest, and the

whole process is the involvement of only two oxygen ions. The proton transfer in the cd process is more difficult due to the limitation of distance. In this paper we choose the paths in Fig. 4b and Fig. 4c as representative paths in order to ensure the continuity in the proton diffusion process. Path I and path II have each 7 migration steps (a-h), both consisting of three-steps of proton transfer and four-steps of proton rotation.

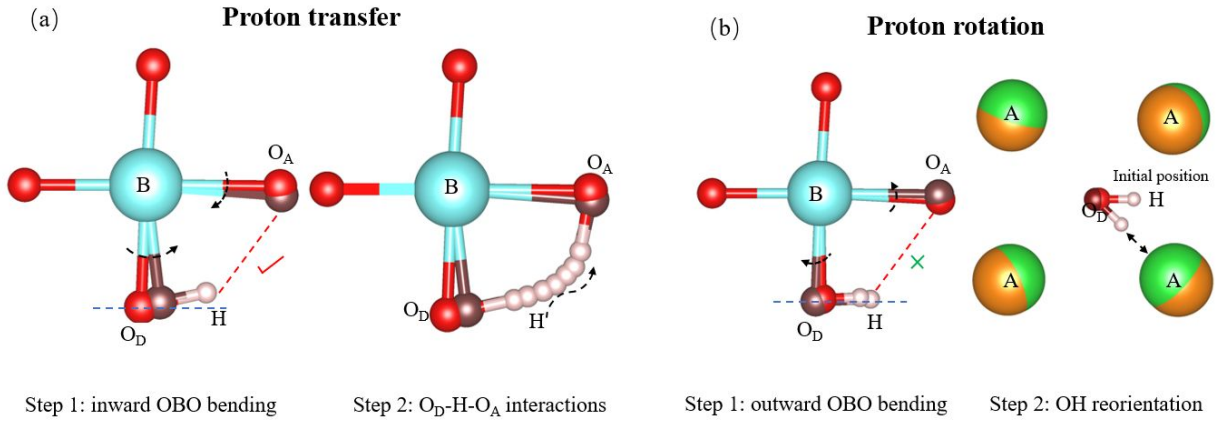

Figure 3: Schematic diagram of the proton diffusion mechanism in ABO_3 perovskite oxides. (a) Description of the proton transfer process: inward OBO bending motion and O_D-H-O_A interaction in the BO_2 plane; (b) Description of proton rotation process: outward OBO bending motion and reorientation of hydroxide ions in the AO plane. The check mark in the diagram indicates that proton interact between O_D and O_A. The cross indicates that protons do not interact between O_D and O_A.

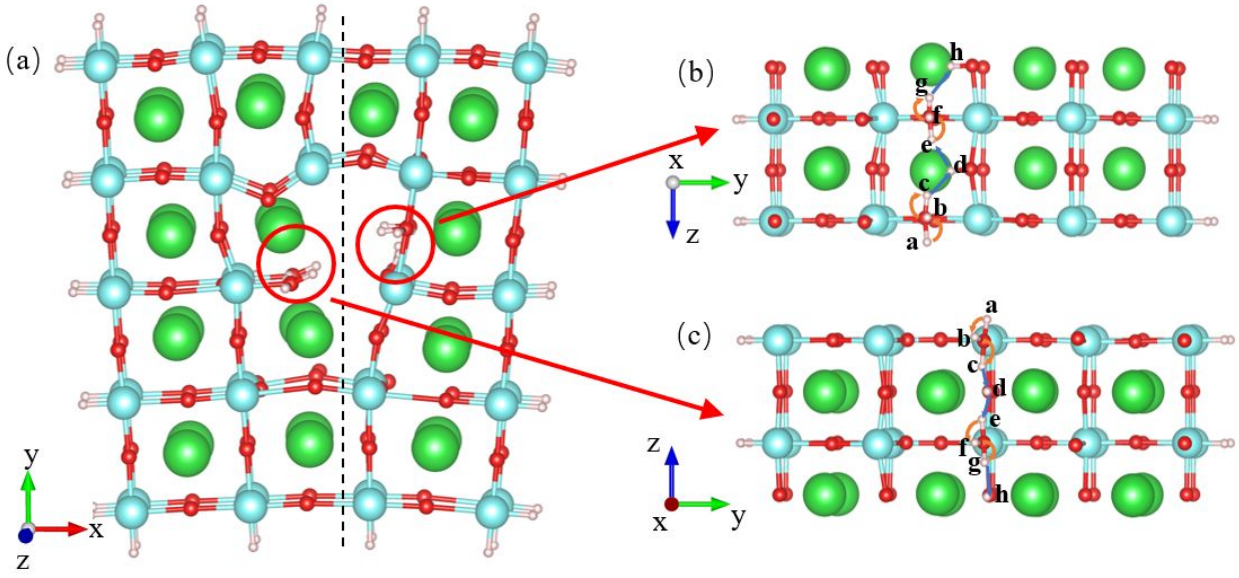

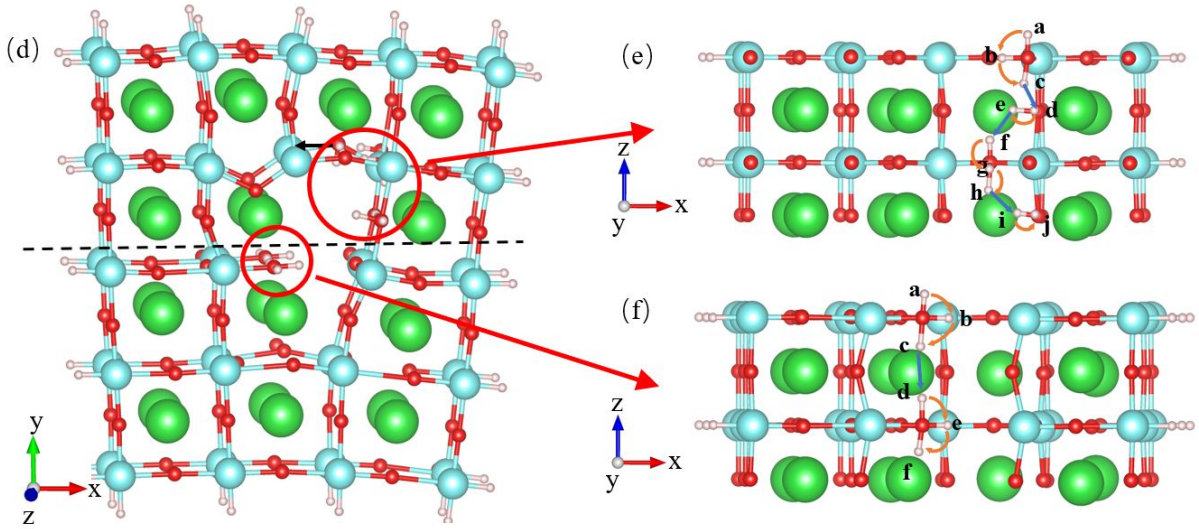

Figure 4: The proton conduction path on the dislocation core. They are shown in detail in (b) path I, (c) path II, (e) path III and (d) path IV, respectively.

In order to understand more clearly the migration mechanism of protons in BZY-D, the minimum migration energy paths of protons in the dislocation core is calculated using the NEB method. Using the initial position of path I (binding point a) as the reference point, the energies of the binding points and transition states of the protons in the two migration paths in BZY-D were calculated, as shown in Fig.5. The maximum energy barriers in proton migration path I and path II are 0.50 eV (de) and 0.64 eV (cd), respectively, as seen in Fig.5. With respect to the energy barrier value in bulk BZY (0.2 eV)[70], it is much larger for the proton diffusion in the dislocation core. According to Arrhenius' law, the rate of particle transport is proportional to the term $\exp(-E_{barrrier}/k_BT)$, where T(absolute temperature) and k_B (Boltzmann's constant) are constant, so the larger the energy barrier $E_{barrier}$ the slower the particle diffusion rate, which means that the proton diffusion rate becomes slower in the dislocation compared to in the bulk. The results are similar to those of other solid oxides such as $SrTiO_3$ and CeO_2, where the oxide ion diffusion is hindered by the dislocation defects and the conductivity of the ions is reduced [17-19]. This suggests that the proton conduction in the dislocation core plays a key role in the overall proton transport in $BaZrO_3$ crystals. It can be seen from the fig.5 that when the proton diffuses from a to h, the maximum energy barrier is on path II and proton diffusion prefers to occur in path I. When the proton diffuses from h to a, the maximum energy barrier is on path I at this time and path II is the most favorable diffusion path.

As shown in Fig.5, the proton has a minimum relative energy of -0.72 eV at the d site on path I. The migration barrier at the cd stage on path I is 0.179 eV, indicating that the proton can easily diffuse to the lowest energy point in the dislocation core. The migration barrier for the proton jumping out of the energy minimum is much higher (0.54 eV for the de step on path I), resulting in the proton being more easily trapped in the dislocation core. It can be seen that the proton is more stable at the d site of path I. Next, we analyze the proton trapping mechanism in the dislocation core by comparison different local atomic structures.

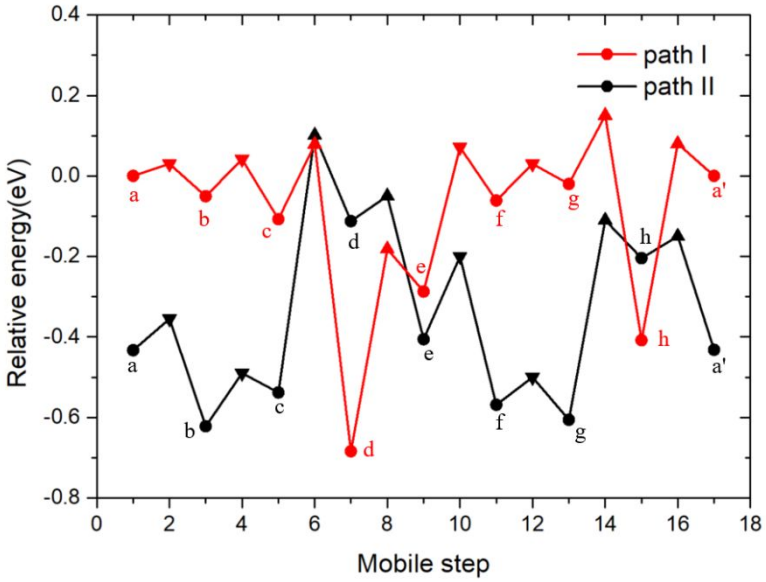

Figure 5: The relative energies of binding site and transition state of the protons in the two diffusion paths. The upper triangle is the transition state energy during proton transfer and the lower triangle is the transition state energy during proton rotation. The remaining points are the relative energies of the binding points. a' is the position in the periodic structure corresponding to a.

3.2. Proton trapping in dislocation core

In order to understand the high stability of protons at the d site of path I, we considered the hydrogen bond configuration of oxygen ion in the local structure. In addition, we calculated the Voronoi volume for several representative structures, which represents the available space for each atom and which is only affected by the nearest atom around the target atom. Fig.6 shows calculations for typical O-H stable conformations of oxygen ions in dislocations and bulk. O1 is located in the bulk structure, O2 is located in the maximum Voronoi volume in the dislocation core, O3 is located in the lowest energy in the dislocation core and O4 is similar to O3 in structure. As shown in the partial enlargement of O1, in the perfect bulk structure, the bond length of O-H is 0.99 Å. The proton is located between the bound oxygen ion and two neighboring Ba ions [36, 57]. At this position, the proton is farthest away from the surrounding Ba and Zr ions, resulting in the least Coulomb repulsion. It is clearly seen in the local magnification of O2, O3 and O4 that there is a significant local lattice deformation owing to the presence of protons. The Voronoi volume of O2 (24.038 $Å^3$), O3 (23.715 $Å^3$) and O4 (21.546 $Å^3$) in the dislocation core are larger than those of O1 (15.102 $Å^3$), which favors the residence of protons in these positions. The protons on the dislocation core prefer locations with more free space to decrease the repulsive forces of nearby Ba and Zr ions.

Furthermore, we have analyzed the hydrogen bond configuration in the local structure in detail. In the hydrogen bonds structure, the shorter the bond length, the stronger the hydrogen bond is when the bond angle is close to 180°. In the hydrogen bond configuration of O1, a symmetric nonlinear hydrogen bond configuration is formed with a bond angle of 120° and a bond length of 2.25 Å, and this is in agreement with the results of reference [71]. In the hydrogen bond configuration of O2, the oxygen is in a suspended bond state and the O-H bond formed over it is unstable. In the hydrogen bonding configuration of O3 and O4, two symmetrical nonlinear hydrogen bonds are formed, and compared to the hydrogen bonds of O1 and O4, the bond length on O3 is larger (2.44 Å) and the bond angle is similar (110°). This implies that the combined effect of free space and local hydrogen bond configuration results in high stability of protons at the lowest energy point (O3) position.

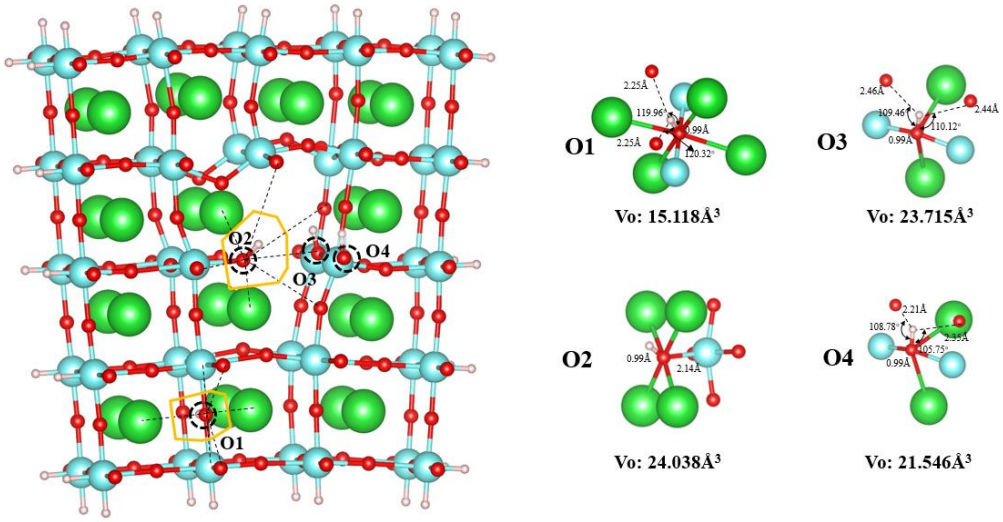

Figure 6: The hydrogen bond configurations near O1, O2, O3 and O4. The dashed line between H and O atoms in the local structure indicates hydrogen bonding. Vo indicates the Voronoi volume in the vicinity of the oxygen ion. The area enclosed by the yellow solid line is a schematic of the Voronoi volumes of O1 and O2 (O2, O3 and O4 are similar).

3.3 Activation energy of proton diffusion in dislocation core

In this section we focus on the sources of energy barriers in the proton diffusion process and study two representative diffusion processes in detail. In the proton transfer process (cd in path I), we divide the whole proton transfer process into three independent steps (Fig.7a, 7b and 7c), taking the structure at point c as the initial state (relative energy of 0). In the proton rotation process (bc in path I), we divide the whole proton rotation process into three independent steps (Fig.7d, 7e and 7f), taking the structure at point b as the initial state (relative energy is 0).

From the above calculations, it is obtained that the d site in path I has the smallest relative energy and the most stable proton structure. To explain the origin of the minimum activation energy, we performed a detailed analysis of the proton transfer process (cd) near the d site. Combined with the previous analytical calculations for BZY and BZY-GB[70, 72], we analyzed the local structural deformation among the initial structure, saddle structure and final structure during the proton transfer of BZY-D to obtain the three basic steps of proton transfer: inward O-B-O motion, O_D-H-O_A interaction and O-B-O bending recovery. The relative energies of these three fundamental steps are given in Fig.7a-Fig.7c. The horizontal coordinate, relative O-B-O angle, represents the actual angle change of the O-B-O angle. O-B-O angle is bent inward and the angle decreases, which is denoted as negative; O-B-O angle is bent outward and the angle increases, which is denoted as positive. For the reaction coordinate in Fig. 7b, we consider the position change of the proton in the O_D-H-O_A interaction as a unit, and the horizontal coordinate represents the relative position of the proton during the movement, which is a normalized value. The maximum energy barrier during O-B-O motion is given as 0.132 eV in Fig.7a ($\angle O_D B O_A$ in the inset), which involves lattice deformation on the local structure. The energy barrier of the O_D and O_A interaction is maximum (0.047 eV) at the intermediate position between O_D and O_A for proton is given in Fig.7b. The relative energy changes during the O-B-O relaxation is given in Fig.7c, where the energy barrier does not occur throughout the process. It can be noted that in the proton transfer of step cd of path I, the total energy barrier of the two first steps obtained by the decomposition is 0.179 eV, which is equal to the calculation of NEB, indicating that the

source of the total energy barrier is associated with O-B-O motion and O_D-H-O_A interaction. This is similar to the proton transfer calculated in BZY and BZY-GB, further verifying the applicability of our proposed three-steps theory. In addition, the energy barrier for the O-B-O motion is greater in BZY-D compared to BZY (0.132 eV for BZY-D and 0.122 eV for BZY), whereas the O_D-H-O_A interactions are reversed (0.047 eV for BZY-D and 0.072 eV for BZY). We will analyze this phenomenon in detail using bond deformation and electron density distribution in later sections. Furthermore, we find that in BZY and BZY-D, the energy barrier for O-B-O motion is larger than that for O_D-H-O_A interaction, implying that the local lattice deformation significantly affects proton transfer process.

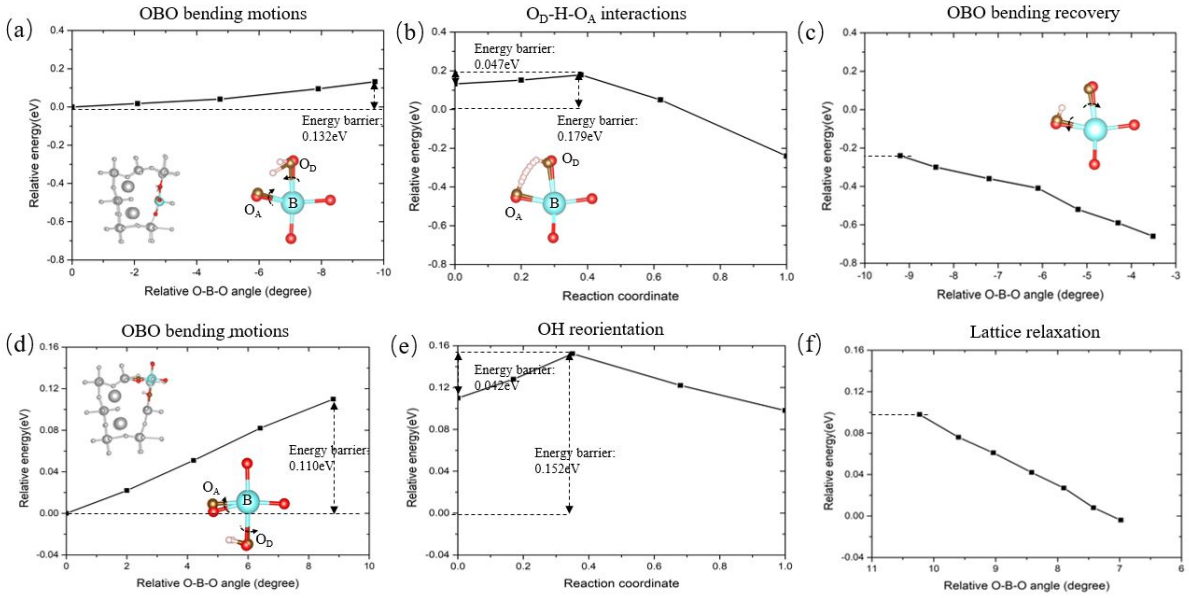

Figure 7: Three decomposition processes of proton transfer and rotation with relative energies. (a) Inward O-B-O motion. (b) O_D-H-O_A interaction. (c) Recovery of O-B-O motion. (d) Outward O-B-O motion. (e) Redirection of the hydroxide ion. (f) Lattice relaxation. The inset shows the deformation process of the structure. The gray ball represents the protons, and the red and brown balls represent the initial structure position and the position after deformation, respectively.

In order to compare with the proton transfer process, we investigated in depth the activation energy origin of proton rotation at the bc step of path I. Combining the previous analytical calculations for BZY and BZY-GB [70, 72], we analyzed the local structural deformation among the initial structure, saddle structure and final structure during the rotation of the hydroxide ion of BZY-D and obtained three basic steps: outward O-B-O motion, reorientation of the hydroxide ion and lattice relaxation. In Fig.7d-Fig.7f the relative energies of these three fundamental steps are given. For the reaction coordinate in Fig. 7e, we consider the angular change of proton rotation in hydroxide ion reorientation as a unit, and the horizontal coordinate represents the relative position of the proton during the rotation, which is a normalized value. Fig.7d gives the relative energy in the O-B-O motion ($\angle O_D B O_A$ in the inset), and the maximum energy barrier for lattice deformation is 0.110 eV. The relative energy for the reorientation of the hydroxide ion is given in Fig.7e (energy barrier is 0.042 eV). The relative energy changes during the lattice relaxation is given in Fig.7f, where the energy barrier does not occur throughout the process. It can be noted that in the proton rotation of step bc of path I, the total energy barrier of the two first steps obtained by the decomposition is 0.152 eV, which is similar to the calculation of NEB

(0.154 eV), indicating that the source of the total energy barrier is associated with O-B-O motion and hydroxide ion reorientation, while provides more clarity on the source of activation energy for the proton rotation process. In addition, the energy barrier of the O-B-O motion in BZY-D is larger compared to BZY (0.269 eV in BZY-D and 0.109 eV in BZY), and the same is true for the hydroxide ion reorientation (0.354 eV in BZY-D and 0.083 eV in BZY), a phenomenon that will be described in detail in the next section on bonding deformation and electron density distribution. Furthermore, we find that the energy barrier for O-B-O motion is larger than the energy potential for hydroxide ion reorientation in BZY and BZY-D, which implies that the lattice deformation plays a rather important part during proton rotation.

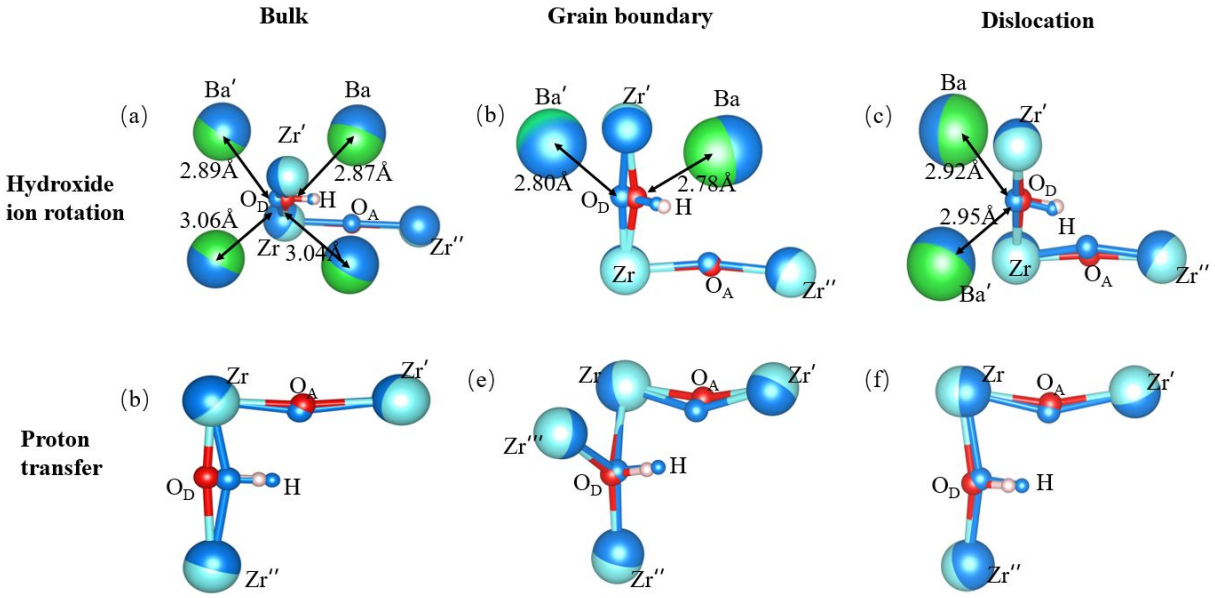

Figure 8: Comparison of structural changes before and after O-B-O motion. Proton rotation in BZY, BZY-GB and BZY-D are indicated in (a), (b), (c); proton transfer in BZY, BZY-GB and BZY-D are indicated in (d), (e), (f). The blue balls and clubs represent the position after the bending motion.

3.4. Effect of dislocation core on proton migration

From the decomposition of BZY and BZY-D in proton transfer and rotation, we observed that O-B-O motion process in BZY-D has a greater relative energy. To understand more clearly the properties of proton transfer and rotation in BZY-D, we compared the effects of bond deformation on O-B-O motion in BZY-D and previously studied BZY[70] and BZY-GB[72]. The structural changes in O-B-O motion during proton migration in BZY, BZY-GB and BZY-D are given in Fig.8. We analyzed the properties of lattice deformation by calculating the bond order. Table 2 and Table 3 summarize the bond order variations of O-B-O motion (bond order variations between the initial and final positions of O-B-O motion) with energy barriers of proton rotation or proton transfer during O-B-O motion in BZY, BZY-GB and BZY-D, respectively. When the value of bond order difference is negative, the bond length increases and the bond strength decreases. For proton transfer or rotation, it can be found that the energy barrier of O-B-O motion is smaller in BZY and BZY-D, and the bond order difference sum is smaller, while the energy barrier of O-B-O motion is larger in BZY- GB, and the bond order difference sum is larger. It can be seen from Table 2 that bond order changes in proton rotation process are focused on O_D-Ba and O_D-Ba'. The oxygen ion in BZY has four Ba ions evenly distributed around it and is subject to more uniform interactions , while

in both BZY-GB and BZY-D the oxygen ion is subject to two A ions, and the oxygen ion is closer to the A ion, but the proton in BZY-GB is more biased toward the Ba ion, resulting in stronger interactions. Therefore, the increase in the energy barrier during O-B-O motion is due to the increase in the binding strength between O-A, which hinders the rotation of the hydroxide ion. From Table 3, it can be seen that the bond order changes are mainly focused on $O_D-\mathrm{Zr}$,O_D-Zr'' and O_D-Zr'''.during the proton transfer process. Compared to the two O-Zr bonds in the oxygen donor structures of BZY and BZY-D, there is an additional O-Zr bond interaction in BZY-GB. The increase in the number of O and Zr ions and bond strength in the GB structure leads to an increase in the energy barrier for local lattice deformation, which hinders the proton transfer in the GB.

Table 2
Bond order changes in O-B-O motion in proton rotation process.

System	Barrier(eV)	Bond order differences						Sum
		O_D—Zr	O_D—Zr'	O_A—Zr	O_A—Zr''	O_D—Ba	O_D—Ba'	
BZY	0.109	-0.002	-0.005	0.012	-0.022	0.014	0.012	0.009
BZY-GB	0.269	0.008	-0.011	0.025	-0.030	0.064	0.057	0.113
BZY-D	0.110	0.003	-0.008	0.016	-0.035	0.021	0.016	0.013

Table 3
Bond order changes in O-B-O motion in proton transfer process.

System	Barrier(eV)	Bond order differences					Sum
		O_D—Zr	O_D—Zr''	O_D—Zr'''	O_A—Zr′	O_A—Zr	
BZY	0.122	0.056	-0.072		-0.026	0.060	0.018
BZY-GB	0.233	0.037	-0.033	0.028	-0.038	0.073	0.067
BZY-D	0.132	0.048	-0.052		-0.034	0.063	0.025

We next investigated the valence electron density distribution of local atoms in the vicinity of O_D-H-O_A interactions and hydroxide ion reorientation in BZY, BZY-GB, and BZY-D (Fig.9). Fig.9a illustrates the electron density distribution near the hydroxide ion reorientation. The bond lengths of the hydroxide ions in BZY-GB and BZY-D increase from 0.978 Å in BZY to 0.985 Å and 0.979 Å, respectively, since there are only two O-A bond interactions in BZY-GB and BZY-D, this provides a larger proton free space. Moreover, the bond strength of O-A gradually decreases in BZY-GB, BZY and BZY-D (O-Ba bond lengths of 2.816 Å, 3.423 Å and 3.668 Å, respectively). Therefore, the stronger O-A bond in BZY-GB inhibits the reorientation of the hydroxide ion and produces a larger energy barrier (0.354eV), while the energy barrier for hydroxide ion reorientation in BZY-D is much smaller (0.042eV). In summary, the strength of the O-A bond controls the energy barrier for the reorientation of the hydroxide ion. Fig.9b shows the electron density distribution around O_D-H-O_A interaction in proton transfer process. The presence of three O-A bonds in BZY-GB reduces the Voronoi volume near O. In BZY-D, similar to the structure in BZY, but the presence of the dislocation core leads to an increase in the Voronoi volume near the O_D-H-O_A interactions. The larger Voronoi volume on the local structure reduces the proton binding strength to the oxygen donor (1.023 Å, 1.029 Å and 1.050 Å for BZY-GB, BZY and BZY-D, respectively), which leads to easier proton movement from the oxygen donor to the oxygen acceptor and facilitates proton transfer, leading to a smaller energy barrier to O_D-H-O_A interactions.

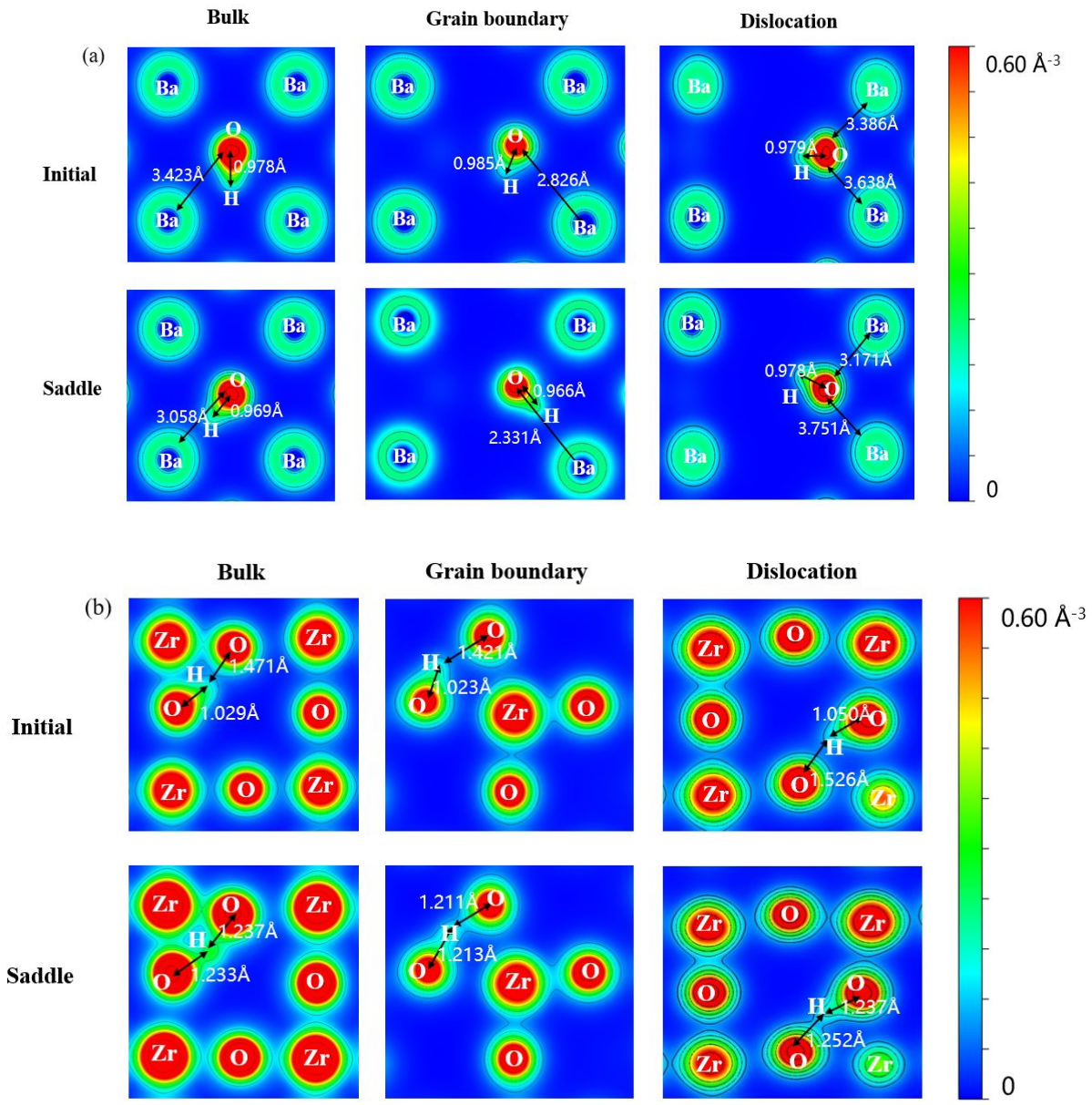

Figure 9: Electronic density distribution of the local structures of (a) hydroxide ion reorientation in proton rotation and (b) O_D-H-O_A interaction in proton transfer.

4. conclusions

We have investigated the process and mechanism of proton crossing through the dislocation core in $BaZrO_3$ by writing stub code using the multiscale simulation theory of QM/MM in combination with LAMMPS and VASP packages. We find that there is proton capture at the dislocation core, and this results in a higher energy barrier for proton crossing the dislocation. Meanwhile, the origin of activation energy for proton migration in BZY-D was analyzed in comparison with the previously proposed "three-steps" method of proton transfer and rotation, and the local lattice deformation was found to have an important effect in proton diffusion processes.

The proton diffusion in the dislocation core has a significant capture effect, in order to minimize the Coulomb effect of nearby cations, the proton prefers to stay at the position with larger free space. Meanwhile, As the O-H bond formed is more stable, the stronger the hydrogen bonding effect and the more easily the proton is trapped. In addition, in the perovskite type materials with edge dislocation defects, there is no dislocation-pipeline effect formed to accelerate the ion transfer, and the edge dislocation defects instead reduce the proton diffusion. During the proton transfer, the local configuration between the oxygen ion and the surrounding B ion significantly affects the O-B-O motion, and as the number of O_D-Zr bonds increases the interactions to which the oxygen donor is subjected, the local lattice deformation is suppressed. During the O_D-H-O_A interaction, the larger bond length of O_D -H facilitates proton transfer, resulting in a smaller energy barrier for the whole process. For the proton rotation process, the presence of grain boundaries and dislocation defects leads to a larger free space for the proton migration process, and although this facilitates the small angle proton rotation , the bond strength among the oxygen and the adjacent Ba ions is strong enough that the protons need to overcome these interactions to achieve the reoriented motion of the hydroxide ion. In this paper, the diffusion mechanism of protons on the dislocation core of $BaZrO_3$ is described at the atomic level, which is a guideline for further improvement of the proton diffusion properties of the material.

Acknowledgements

This work is supported by the National Science Foundation of China under Grant No. 12172112, 11932005, and 11974091, and the International Postdoctoral Exchange Fellowship Program of China under Grants No. 20140016, the National Science Foundation under grant # 1545907, the National Center for Supercomputing Applications (NCSA).

References

[1] Y. Yamazaki, F. Blanc, Y. Okuyama, L. Buannic, J.C. Lucio-Vega, C.P. Grey, S.M. Haile, Proton trapping in yttrium-doped barium zirconate, Nature Materials, 12 (2013) 647-651.
[2] L. Malavasi, C.A. Fisher, M.S. Islam, Oxide-ion and proton conducting electrolyte materials for clean energy applications: structural and mechanistic features, Chem Soc Rev, 39 (2010) 4370-4387.
[3] W. Zajac, D. Rusinek, K. Zheng, J. Molenda, Applicability of Gd-doped BaZrO3, SrZrO3, BaCeO3 and SrCeO3 proton conducting perovskites as electrolytes for solid oxide fuel cells, Cent Eur J Chem, 11 (2013) 471-484.
[4] T. Kuroha, K. Yamauchi, Y. Mikami, Y. Tsuji, Y. Niina, M. Shudo, G. Sakai, N. Matsunaga, Y. Okuyama, Effect of added Ni on defect structure and proton transport properties of indium-doped barium zirconate, International Journal of Hydrogen Energy, 45 (2020) 3123-3131.
[5] D.L. Han, T. Uda, The best composition of an Y-doped BaZrO3 electrolyte: selection criteria from transport properties, microstructure, and phase behavior, Journal of Materials Chemistry A, 6 (2018) 18571-18582.
[6] M. Legros, G. Dehm, E. Arzt, T.J. Balk, Observation of giant diffusivity along dislocation cores, Science, 319 (2008) 1646-1649.
[7] Y. Yamazaki, R. Hernandez-Sanchez, S.M. Haile, High Total Proton Conductivity in Large-Grained Yttrium-Doped Barium Zirconate, Chemistry of Materials, 21 (2009) 2755-2762.
[8] F. Iguchi, T. Yamada, N. Sata, T. Tsurui, H. Yugami, The influence of grain structures on the electrical conductivity of a BaZr0.95Y0.05O3 proton conductor, Solid State Ionics, 177 (2006) 2381-2384.
[9] I. Oikawa, H. Takamura, Correlation among Oxygen Vacancies, Protonic Defects, and the Acceptor Dopant in Sc-Doped BaZrO3 Studied by 45Sc Nuclear Magnetic Resonance, Chemistry of Materials, 27 (2015) 6660-6667.
[10] C.W. Mburu, S.M. Gaita, C.S. Knee, M.J. Gatari, M. Karlsson, Influence of Yttrium Concentration on Local Structure in BaZr1−xYxO3−δ Based Proton Conductors, The Journal of Physical Chemistry C, 121 (2017) 16174-16181.
[11] D. Noferini, M.M. Koza, M. Karlsson, Localized Proton Motions in Acceptor-Doped Barium Zirconates, The Journal of Physical Chemistry C, 121 (2017) 7088-7093.
[12] F. Iguchi, N. Sata, T. Tsurui, H. Yugami, Microstructures and grain boundary conductivity of BaZr1−xYxO3 (x=0.05, 0.10, 0.15) ceramics, Solid State Ionics, 178 (2007) 691-695.

[13] M.S. Islam, P.R. Slater, J.R. Tolchard, T. Dinges, Doping and defect association in AZrO(3) (A = Ca, Ba) and LaMO(3) (M = Sc, Ga) perovskite-type ionic conductors, Dalton Trans, (2004) 3061-3066.
[14] M.E. Björketun, P.G. Sundell, G. Wahnström, Effect of acceptor dopants on the proton mobility inBaZrO3: A density functional investigation, Physical Review B, 76 (2007) 054307.
[15] B. Merinov, W. Goddard, 3rd, Proton diffusion pathways and rates in Y-doped BaZrO3 solid oxide electrolyte from quantum mechanics, J Chem Phys, 130 (2009) 194707.
[16] N. Kitamura, J. Akola, S. Kohara, K. Fujimoto, Y. Idemoto, Proton Distribution and Dynamics in Y- and Zn-Doped BaZrO3, The Journal of Physical Chemistry C, 118 (2014) 18846-18852.
[17] K.P. Song, H. Schmid, V. Srot, E. Gilardi, G. Gregori, K. Du, J. Maier, P.A. van Aken, Cerium reduction at the interface between ceria and yttria-stabilised zirconia and implications for interfacial oxygen non-stoichiometry, Apl Materials, 2 (2014) 032104.
[18] C.P. Chang, M.W. Chu, H.T. Jeng, S.L. Cheng, J.G. Lin, J.R. Yang, C.H. Chen, Condensation of two-dimensional oxide-interfacial charges into one-dimensional electron chains by the misfit-dislocation strain field, Nature Communications, 5 (2014) 1-8.
[19] L.F. Wang, Z. Xu, W.L. Wang, X.D. Bai, Atomic Mechanism of Dynamic Electrochemical Lithiation Processes of MoS2 Nanosheets, Journal of the American Chemical Society, 136 (2014) 6693-6697.
[20] E. Wachsman, T. Ishihara, J. Kilner, Low-temperature solid-oxide fuel cells, Mrs Bull, 39 (2014) 773-782.
[21] L.X. Sun, D. Marrocchelli, B. Yildiz, Edge dislocation slows down oxide ion diffusion in doped CeO2 by segregation of charged defects, Nature Communications, 6 (2015) 1-10.
[22] P.P. Dholabhai, G. Pilania, J.A. Aguiar, A. Misra, B.P. Uberuaga, Termination chemistry-driven dislocation structure at SrTiO3/MgO heterointerfaces, Nature Communications, 5 (2014) 1-7.
[23] V. Metlenko, A.H.H. Ramadan, F. Gunkel, H.C. Du, H. Schraknepper, S. Hoffmann-Eifert, R. Dittmann, R. Waser, R.A. De Souza, Do dislocations act as atomic autobahns for oxygen in the perovskite oxide SrTiO3?, Nanoscale, 6 (2014) 12864-12876.
[24] K.P. McKenna, Electronic and Chemical Properties of a Surface-Terminated Screw Dislocation in MgO, Journal of the American Chemical Society, 135 (2013) 18859-18865.
[25] S.T. Murphy, E.E. Jay, R.W. Grimes, Pipe diffusion at dislocations in UO2, J Nucl Mater, 447 (2014) 143-149.
[26] W.A. Curtin, D.L. Olmsted, L.G. Hector, A predictive mechanism for dynamic strain ageing in aluminium-magnesium alloys, Nature Materials, 5 (2006) 875-880.
[27] M. Legros, G. Dehm, E. Arzt, T.J. Balk, Observation of giant diffusivity along dislocation cores, Science, 319 (2008) 1646-1649.
[28] C.L. Jia, A. Thust, K. Urban, Atomic-scale analysis of the oxygen configuration at a SrTiO3 dislocation core, Phys Rev Lett, 95 (2005) 225506.
[29] D. Marrocchelli, L. Sun, B. Yildiz, Dislocations in SrTiO3: easy to reduce but not so fast for oxygen transport, J Am Chem Soc, 137 (2015) 4735-4748.
[30] L. Sun, D. Marrocchelli, B. Yildiz, Edge dislocation slows down oxide ion diffusion in doped CeO(2) by segregation of charged defects, Nat Commun, 6 (2015) 6294.
[31] Y.H. Jing, H. Matsumoto, N.R. Aluru, Mechanistic Insights into Hydration of Solid Oxides, Chemistry of Materials, 30 (2018) 138-144.
[32] H.W. Niu, Y.H. Jing, Y. Sun, L.C. Guo, N.R. Aluru, W.Q. Li, J.Q. Yang, X.J. Li, On the anomalous diffusion of proton in Y-doped BaZrO3 perovskite oxide, Solid State Ionics, 376 (2022).
[33] H.W. Niu, Y.H. Jing, Y. Sun, L.C. Guo, N.R. Aluru, W.Q. Li, J.Q. Yang, X.J. Li, Strain-induced tunable energy barrier of proton diffusion in Y-doped BaCeO3 and Y-doped BaZrO3, Int J Energ Res, 46 (2022) 7816-7824.
[34] J.H. Yang, D.H. Kim, B.K. Kim, Y.C. Kim, High activation energy for proton migration at Sigma 3(111)/[1(1)over-bar-0] tilt grain boundary in barium zirconate, Solid State Ionics, 252 (2013) 126-131.
[35] M. Saiful Islam, Ionic transport in ABO3 perovskite oxides: a computer modelling tour, Journal of Materials Chemistry, 10 (2000) 1027-1038.
[36] M. Schie, A. Marchewka, T. Muller, R.A. De Souza, R. Waser, Molecular dynamics simulations of oxygen vacancy diffusion in SrTiO3, J Phys Condens Matter, 24 (2012) 485002.
[37] S.J. Stokes, M.S. Islam, Defect chemistry and proton-dopant association in BaZrO3 and BaPrO3, Journal of Materials Chemistry, 20 (2010) 6258-6264.
[38] S.P. Waldow, R.A. De Souza, Computational Study of Oxygen Diffusion along a[100] Dislocations in the Perovskite Oxide SrTiO3, ACS Appl Mater Interfaces, 8 (2016) 12246-12256.
[39] P. Hirel, P. Carrez, E. Clouet, P. Cordier, The electric charge and climb of edge dislocations in perovskite oxides: The case of high-pressure MgSiO3 bridgmanite, Acta Materialia, 106 (2016) 313-321.
[40] N. Choly, G. Lu, W. E, E. Kaxiras, Multiscale simulations in simple metals: A density-functional-based methodology, Physical Review B, 71 (2005) 094101.
[41] Y. Liu, G. Lu, Z.Z. Chen, N. Kioussis, An improved QM/MM approach for metals, Modelling and Simulation in Materials Science and Engineering, 15 (2007) 275-284.
[42] J.L. Gao, Perspective on "Theoretical studies of enzymic reactions: dielectric, electrostatic and steric stabilization of the carbonium ion in the reaction of lysozyme" - Warshel A, Levitt M (1976) J Mol Biol 103 : 227-249, Theor Chem Acc, 103 (2000) 328-329.

[43] J. Kussmann, M. Beer, C. Ochsenfeld, Linear-scaling self-consistent field methods for large molecules, Wires Comput Mol Sci, 3 (2013) 614-636.
[44] L. Delle Site, C. Holm, N.F.A. van der Vegt, Multiscale Approaches and Perspectives to Modeling Aqueous Electrolytes and Polyelectrolytes, Multiscale Molecular Methods in Applied Chemistry, 307 (2012) 251-294.
[45] F.J. Keil, Multiscale Modelling in Computational Heterogeneous Catalysis, Multiscale Molecular Methods in Applied Chemistry, 307 (2012) 69-107.
[46] L.C. Menikarachchi, J.A. Gascon, QM/MM Approaches in Medicinal Chemistry Research, Curr Top Med Chem, 10 (2010) 46-54.
[47] K. Meier, A. Choutko, J. Dolenc, A.P. Eichenberger, S. Riniker, W.F. Van Gunsteren, Multi-resolution simulation of biomolecular systems: a review of methodological issues, Angewandte Chemie International Edition, 52 (2013) 2820-2834.
[48] H.M. Senn, W. Thiel, QM/MM methods for biological systems, Top Curr Chem, 268 (2007) 173-290.
[49] G. Groenhof, Introduction to QM/MM simulations, Biomolecular Simulations, (2013) 43-66.
[50] S. Pezeshki, H. Lin, Recent developments in QM/MM methods towards open-boundary multi-scale simulations, Mol Simulat, 41 (2015) 168-189.
[51] W. Zhao, Q.Y. Meng, L.J. Yang, C.Y. Wang, DIFFUSION OF LITHIUM IN SILICON AFFECTED BY 60 degrees MISFIT-DISLOCATION, Mod Phys Lett B, 27 (2013) 1350168.
[52] C.Y. Wang, L.J. Yang, W. Zhao, Q.Y. Meng, C.L. Li, G.X. Wu, B.L. Wang, Multi-scale simulation of lithium diffusion in the presence of a 30 degrees partial dislocation and stacking fault in Si, J Appl Phys, 115 (2014) 043532.
[53] C.Y. Wang, C. Zhang, Q.L. Xue, C.L. Li, J.Q. Miao, P.F. Ren, L.J. Yang, Z.L. Yang, Atomic mechanism of the distribution and diffusion of lithium in a cracked Si anode, Scripta Mater, 197 (2021) 113807.
[54] A. Jain, S.P. Ong, G. Hautier, W. Chen, W.D. Richards, S. Dacek, S. Cholia, D. Gunter, D. Skinner, G. Ceder, K.A. Persson, Commentary: The Materials Project: A materials genome approach to accelerating materials innovation, APL Materials, 1 (2013) 011002.
[55] G. Kresse, J. Furthmuller, Efficient iterative schemes for ab initio total-energy calculations using a plane-wave basis set, Physical Review B, 54 (1996) 11169-11186.
[56] G. Kresse, J. Furthmuller, Efficiency of ab-initio total energy calculations for metals and semiconductors using a plane-wave basis set, Computational Materials Science, 6 (1996) 15-50.
[57] G. Kresse, Ab-Initio Molecular-Dynamics for Liquid-Metals, J Non-Cryst Solids, 193 (1995) 222-229.
[58] J.P. Perdew, K. Burke, M. Ernzerhof, Generalized gradient approximation made simple, Physical Review Letters, 77 (1996) 3865-3868.
[59] S.L. Dudarev, G.A. Botton, S.Y. Savrasov, C.J. Humphreys, A.P. Sutton, Electron-energy-loss spectra and the structural stability of nickel oxide: An LSDA+U study, Physical Review B, 57 (1998) 1505-1509.
[60] G. Kresse, D. Joubert, From ultrasoft pseudopotentials to the projector augmented-wave method, Physical Review B, 59 (1999) 1758-1775.
[61] P.E. Blochl, Projector Augmented-Wave Method, Physical Review B, 50 (1994) 17953-17979.
[62] T.S. Bjorheim, A. Loken, R. Haugsrud, On the relationship between chemical expansion and hydration thermodynamics of proton conducting perovskites, Journal of Materials Chemistry A, 4 (2016) 5917-5924.
[63] W. Tang, E. Sanville, G. Henkelman, A grid-based Bader analysis algorithm without lattice bias, J Phys-Condens Mat, 21 (2009) 084204.
[64] G. Henkelman, B.P. Uberuaga, H. Jonsson, A climbing image nudged elastic band method for finding saddle points and minimum energy paths, Journal of Chemical Physics, 113 (2000) 9901-9904.
[65] T.A. Manz, Introducing DDEC6 atomic population analysis: part 3. Comprehensive method to compute bond orders, Rsc Advances, 7 (2017) 45552-45581.
[66] P. Raiteri, J.D. Gale, G. Bussi, Reactive force field simulation of proton diffusion in BaZrO3 using an empirical valence bond approach, J Phys-Condens Mat, 23 (2011) 334213.
[67] S.J. Stokes, M.S. Islam, Defect chemistry and proton-dopant association in BaZrO3 and BaPrO3, Journal of Materials Chemistry, 20 (2010) 6258.
[68] K.D. Kreuer, Proton-conducting oxides, Annual Review of Materials Research, 33 (2003) 333-359.
[69] K.D. Kreuer, Aspects of the formation and mobility of protonic charge carriers and the stability of perovskite-type oxides, Solid State Ionics, 125 (1999) 285-302.
[70] Y.H. Jing, N.R. Aluru, The role of A-site ion on proton diffusion in perovskite oxides (ABO(3)), Journal of Power Sources, 445 (2020) 227327.
[71] A. Lindman, E.E. Helgee, G. Wahnstrom, Comparison of Space-Charge Formation at Grain Boundaries in Proton-Conducting BaZrO3 and BaCeO3, Chemistry of Materials, 29 (2017) 7931-7941.
[72] S.F. Yue, Y.H. Jing, Y. Sun, J.Q. Zhao, N.R. Aluru, Mechanistic insights into proton diffusion in Sigma 3 BaZrO3 (210)[001] tilt grain boundary, Ceram Int, 48 (2022) 2097-2104.